VOL. 13, NO. 9, MAY 2018 ISSN 1819-6608
ARPN Journal of Engineering and Applied Sciences

www.arpnjournals.com

ANALYSIS OF PLAIN ALUMINIUM SATURATION WITH HYDROGEN WHILE ADDING DIFFERENT COMPONENTS

Belyaev S. V.[1], Partyko E. G.[1], Kosovich A. A.[1], Baranov V. N.[1], Bezrukikh A. I.[1], Gubanov I. Y.[1], Gorokhov Y. V.[1], Koptseva N. P.[1], Kirko V. I.[1, 2], Lesiv E. M.[1], Yuryev P. O.[1] and Stepanenko N. A.[1]
[1]Siberian Federal University, Krasnoyarsk, Russia
[2]Krasnoyarsk State Pedagogical University named after Victor Astafijev, Krasnoyarsk, Russia
E-Mail: kopceva63@mail.ru

ABSTRACT

The article contains the results of research into various fluxes and addition alloys applied at aluminum plants in Russia. Fuxes containing crystalline hydrates and hygroscopic water have been shown to be the source of aluminum melt hydrogen saturation. The research resulted in technical solutions aimed at the reduction of hydrogen absorption in aluminium melts with fluxes.

Keywords: fluxes, hydrogen, aluminium, aluminium melt hydrogen saturation, X-ray phase analysis, differential thermal analysis, hygroscopic water, crystal water.

INTRODUCTION

The competitiveness of metal products in the world market is largely determined by their quality. Given the fact that the design of machines and units employs parts made of aluminium and its alloys, the technology for the production of the latter is given particular attention [1]. The aluminium alloys' quality is known to mostly depend on the purity of the metal, in particular, on the content of nonmetallic inclusions, including gas impurities. The main impurity particles are aluminium oxide Al_2O_3 and hydrogen H_2 [2 – 4].

Hydrogen is one of the most significant gaseous impurities featuring an adverse impact on the processing behavior of products made of aluminum and its alloys. Hydrogen dissolved in an aluminum solid solution under particular conditions contributes to the formation of gas and shrinkage porosity, which increases with the concentration of hydrogen in the melt [5].

One of the possible sources of aluminum saturation with hydrogen is fluxes. Fluxes obtained by melting mixture components in electric furnaces followed by their granulation, as well as mechanically mixed powder fluxes, can absorb moisture from the air while stored, causing the formation of crystalline hydrates, as well as the absorption of moisture on the surface of the crystalline compounds. As a result, the moisture content in the fluxes can reach several percent [6].

Another source of hydrogen in aluminium and its alloys can be the event of alloying and additive modification containing metallic magnesium and titanium.

Thus, the objective of the study is to conduct a quantitative analysis of plain aluminium saturation with hydrogen after the introduction of the traditionally used alloying additives into the melt under regulated temperatures and alloying elements concentrations. The selected additives are listed below:

- refining flux Ekoraf-F5;
- refining flux Ekoraf-F1;
- cover-refining flux FPR23;
- tabletted addition alloy Al-80%Ti;
- alloying addition Mn+flux;
- alloying addition Cu+flux;
- alloying addition Fe+flux;
- alloying addition plain Si;
- alloying addition metal Mg;
- addition alloy Al-10%Sr;
- addition alloy Al-5%Ti-1%B.

RESEARCH METHODOLOGY

Research on fluxes and alloying additives containing fluxes was completed via an X-ray phase analysis and thermogravimetry. The phase analysis was conducted using X-ray diffract meter Shimadzu XRD-7000 in Cu Kα radiation (Figure-1). X-ray diffraction photographs were taken on powders within 2θ angles varying from 5º to 70º at a pace of 0.03 degrees, the scanning speed being 1.5 degrees/min. The results were processed using an information retrieval system for X-ray phase identification materials (IR system of PI) combining qualitative and semi quantitative analyses (using the Reference Intensity Ratio (RIR) method).

Thermal analysis was completed using Synchronous Thermal Analyzer SDT Q 600 (Figure-2) combined with the Nicolet 380 FT-IR spectrometer (Figure-3) and the TGA/FT-IR interface (console for analyzing the gas phase). This complex, during the heating of a sample, provides a means to simultaneously obtain data on modification in the weight of the sample, thermal effects in the system, as well as in the composition of the escaping gas phase. Thermograph records were taken

during the sample's heating with a speed of 10 degrees/min in ambient air to a temperature of 300-350°C, the air blowdown speed being 50 ml/min. The weighed quantity of the samples under study (fluxes and alloying additives containing fluxes) was 20 mg.

Figure-1. Diffractometer Shimadzu XRD-7000.

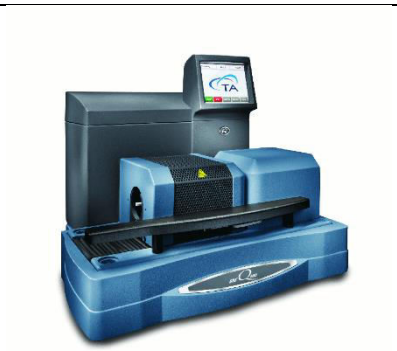

Figure-2. Synchronous thermal analyzer SDT Q 600.

Figure-3. Nicolet 380 FT-IR spectrometer.

The aluminum melt was prepared in induction furnace type IAT 0.06 (induction crucible furnace for aluminium), where 5,000 g of plain A8 aluminum were melt. When the melt reached a temperature of 720°C, a sample of the liquid metal was taken to determine its hydrogen content. The metal temperature was controlled by Pyrometer Testo 835-T2 via the connected thermocouple TC 008 #21-ANXGX.

ALU COMPACT II was applied to determine the change in the hydrogen content in aluminium during its treatment with alloying additives and fluxes. The device is stands out with its compactness, simplicity, and quick testing speed. The hydrogen content was determined using a method in which the "first bubble" emerging from the metal melt is detected.

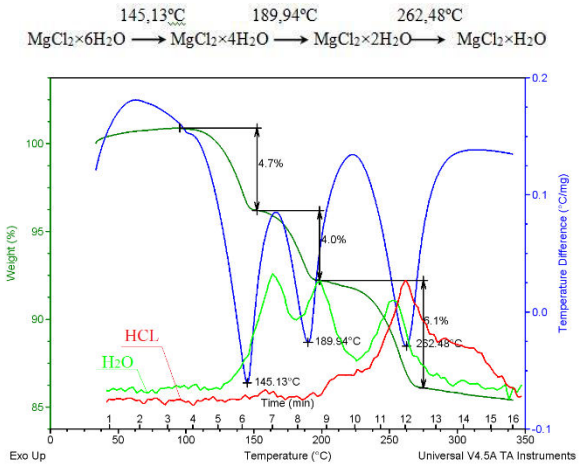

Figure-4. Ekoraf-F5 flux thermogram.

The endothermic effect at 145.13°C is accompanied by the sample's weight loss of 4.7%, which is caused by evaporation of hygroscopic and crystal water from the flux. The endothermic effect at 189.94°C with the sample's weight loss of 4.0% is due to the decomposition of the quadriaqua $MgCl_2 \times 4H_2O$ into dihydrate $MgCl_2 \times 2H_2O$. The endothermic effect corresponding to a temperature of 262.48°C experiences the sample's weight loss in the amount of 6.1 %, which includes the transition of dihydrate $MgCl_2$ into monohydrate $MgCl_2 \times H_2O$ and the formation of hydrogen chloride H Cl as a result of magnesium chloride pyrohydrolisis [7-9].

Total weight loss from the decomposition of Ekoraf-F5 flux up to 300°C amounted to about 14.8%. The high water content in the composition of flux is due to the presence of magnesium chloride crystalline hydrates, which constitute a source of aluminum melt hydrogen absorption.

The hydrogen content in the initial sample of the aluminium melt amounted to 0.19 cm3/100 g. Furthermore, the aluminum was refined using the Ekoraf-F5 flux, with 10 g of it immersed in the metal. After the melt was soaked for 15 min, a sample was taken to detect the hydrogen content. The flux treatment caused increased hydrogen content in the liquid aluminium, totaling 0.38 cm3/100 g Al. The main reason for the increased hydrogen content in the metal is the hygroscopic and crystal water contained in the Ekoraf-F5 flux.

Thermogravimetric studies on the flux were completed to assess the impact of the Ekoraf-F1 flux on the change in the hydrogen content in the aluminium. The Ekoraf-F1 flux thermogram (Figure-5) exhibited two endothermal effects at 154.02°C and 189.94°C. The endothermal effect at 154.02°C is characterized by the sample's weight loss of 18.3%, which was caused by evaporation of mainly crystal water as a flux compound. The endothermal effect at 198.11°C exhibited weight loss in the sample of 9.2%, which was caused by evaporation of the crystal water contained in the flux.

The thermogram curves are identical to the water expulsion process from the carnallite K $MgCl_3 \times 6H_2O$ at atmospheric air pressure. The water expulsion of K $MgCl_3 \times 6H_2O$ is a two-stage process. The first stage includes the decomposition of hexaqua carnallite into dihydrate K $MgCl_3 \times 2H_2O$. This change begins at 105ºC and finishes at 160°C. The second stage is the water expulsion of a dihydrate carnallite to a nonaqueous K $MgCl_3$ and finishes at 215°C. The total weight loss from

the decomposition of Ekoraf-F1 flux up to 300ºC amounted to about 28.5 %. The high content of the crystal water in the flux can have adverse consequences, resulting in the flux turning from a refining agent into a source of the aluminum melt's hydrogen absorption.

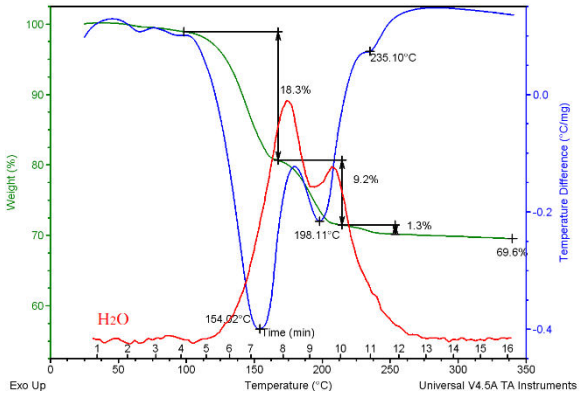

Figure-5. Ekoraf-F1 flux thermogram.

The hydrogen content in the initial aluminium melt sample amounted to 0.21 cm3/100 g. Furthermore, the metal was refined using Ekoraf-F1 flux, with 10 g of it immersed in the metal. When the melt temperature reached 720ºC as well as after 15 min of its soaking, a sample was taken to detect the hydrogen content. The flux treatment caused increased hydrogen content in the liquid aluminium, which totaled 0.29 cm3/100 g Al.

Figure-6 shows the FPR23 flux thermogram. The thermogram did not exhibit any meaningful endothermic and exothermic effects within the temperature scale of up to 350°C. In addition, no vapours were detected coming from the sample, which indicates no hydroscopic or crystal water in the flux content. The total weight loss of the sample up to a temperature of 300°C amounted to 0.6 w%.

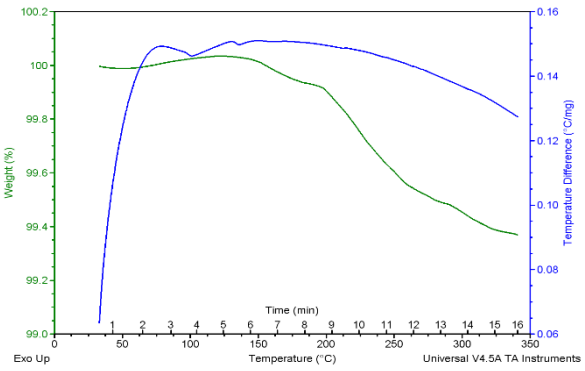

Figure-6. FPR23 flux thermogram

The hydrogen content in the initial aluminium melt sample amounted to 0.21 cm3/100 g. Furthermore, the metal was refined using a FPR23 flux in the amount of 10 g. When the melt temperature reached 720ºC and after 15 min of its soaking, a sample was taken to detect the hydrogen content. The FPR23 flux treatment caused the hydrogen content in the liquid aluminium to be 0.22 cm3/100 g Al.

Experiments were conducted using addition alloy Al-Ti with Ti =80%. The Al-Ti addition alloy thermogram (Figure-7) exhibited an endothermal effect with a maximum of 117.04°C, which was caused by evaporation of hygroscopic water in the amount of 0.8 % w. Further heating of the sample exhibited practically no crystal water contained in the addition alloy. The total weight loss of the sample in the temperature range of up to 350°C amounted to ~1.8%.

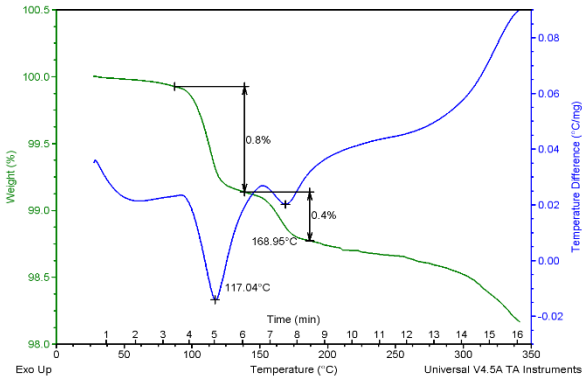

Figure-7. Al-Ti addition alloy thermogram.

The hydrogen content in the initial aluminium melt sample amounted to 0.21 cm3/100 g. Furthermore, an Al-Ti addition alloy was added into the melt in the amount of a 6.25 g equivalent to titanium. When the melt temperature reached 720ºC as well as after 15 min of soaking, a sample was taken to detect the hydrogen content, which amounted to 0.24 cm3/100 g Al. A minor amount of hygroscopic water in the addition alloy resulted in increased hydrogen content in aluminium and amounted to 0.03 cm3/100 g Al.

The experiments were based on the of the tabletted Mn+flux addition alloy with 80%w of manganese and 20%w of a halide-bearing flux. The Mn+flux addition alloy thermogram (Figure-8) exhibited no significant endothermal or exothermal effects. Analysis revealed no water evaporation, which proves the absence of hygroscopic and crystal water in the additive.

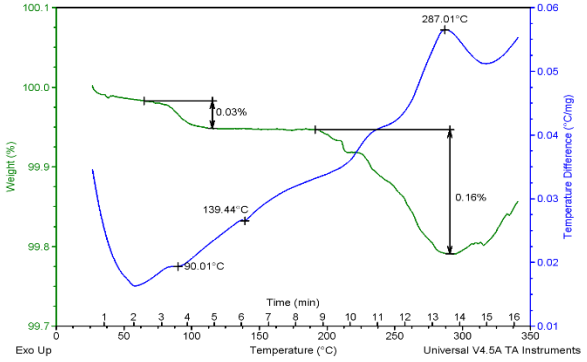

Figure-8. Alloying addition Mn+flux thermogram.

The hydrogen content in the initial sample of the aluminium melt amounted to 0.15 cm^3/100 g. Furthermore, an Mn+flux alloying addition was added into

the melt in the amount of a 1.875 g equivalent to manganese. The estimated content of manganese in the aluminium totaled 0.03%w. When the melt temperature reached 720ºC as well as after 15 min of soaking, a sample was taken to detect the hydrogen content. The hydrogen content in the liquid aluminium after adding the Mn+flux alloying additive amounted to 0.21 cm^3/100 g Al.

The experiments were based on the use of the tabletted Cu+flux addition alloy with 80%w of copper and 20%w of a halide-bearing flux. The Cu+flux addition alloy thermogram (Figure-9) exhibited no significant endothermal or exothermal peaks. The total weight loss of the sample in a temperature range of up to 350°C amounted to ~0.5%. The analysis revealed no water evaporations, which proved the absence of hygroscopic and crystal water in the Cu+flux alloying addition.

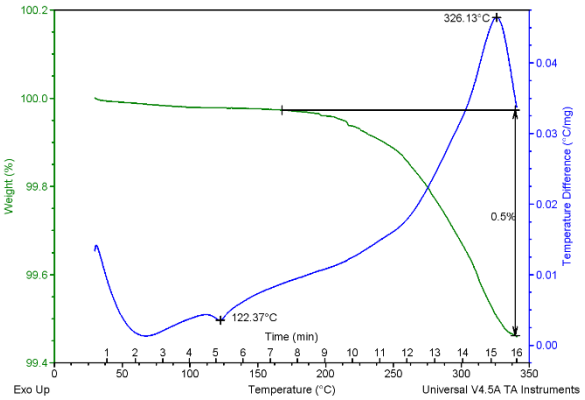

Figure-9. Alloying addition Cu+flux thermogram.

The hydrogen content in the initial sample of the aluminium melt amounted to 0.19 cm3/100 g. Furthermore, a Cu+flux alloying addition was added into the melt in the amount of a 62.5 g equivalent to copper. The estimated copper content in the aluminium totaled 1%w. When the melt temperature reached 720ºC as well as after 15 min of soaking, a sample was taken to detect the hydrogen content. The hydrogen content in the liquid aluminium after adding the Cu+flux alloying additive amounted to 0.20 cm3/100 g Al. Adding the Cu+flux alloying additive into the specified amounts caused an increase in the hydrogen content in the aluminium by 0.01 cm3/100g Al, which is within the measurement error.

The experiments were based on the use of the tabletted Fe+flux addition alloy with the 80%w of iron and 20%w of a halide-bearing flux. The Fe+flux addition alloy thermogram (Figure-10) exhibited no significant endothermal or exothermal effects. The total weight loss of the sample in the temperature range of up to 350°C amounted to ~0.65%w. The analysis revealed no water evaporations, which proved the absence of hygroscopic and crystal water in the alloying addition.

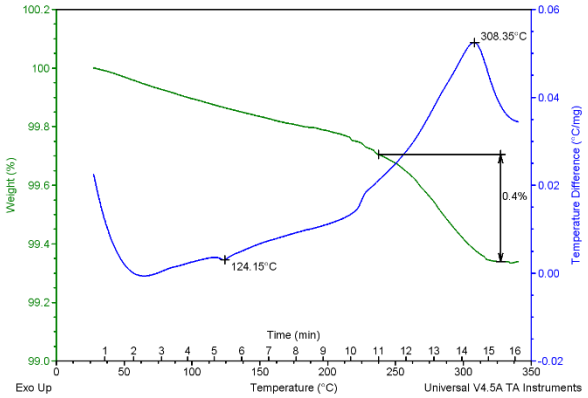

Figure-10. Alloying addition Fe+flux thermogram.

The hydrogen content in the initial sample of the aluminium melt amounted to 0.20 cm^3/100 g. Furthermore, an Fe+flux alloying addition was added into the melt in the amount of a 6.25 g equivalent to iron. The estimated content of iron in the aluminium totaled 0.1%w. When the melt temperature reached 720ºC as well as after 15 min of its soaking, a sample was taken to detect the hydrogen content. The hydrogen content in the liquid aluminium after adding the Fe+flux alloying additive amounted to 0.27 cm3/100 g Al.

In a study of the Si addition, the hydrogen content in the initial sample of the aluminium melt amounted to 0.20 cm^3/100 g Al. Furthermore, an additive of the preliminary heated crystalic Si was added to the melt in an amount equivalent to the silicon content in the metal (7%w). The silicon was heated at 500ºC for 20 min. After the silicon's dilution, when the melt's temperature reached 720ºC, as well as after 15 min of it soaking, a liquid metal sample was taken to detect the hydrogen content. The hydrogen content in the aluminium, after adding the plain silicon, amounted to 0.25 cm^3/100 g Al. The increased hydrogen content in the aluminium and silicon melt is explained by the fact that silicon increases hydrogen solubility in the aluminium melt.

After a study of the Mg addition, the hydrogen content in the initial sample of the aluminium melt amounted to 0.15 cm^3/100 g. Furthermore, the metal Mg additive was added to the melt in an amount equivalent to the magnesium content in the metal (0.3%w). After the magnesium's dilution, when the melt temperature reached 720ºC, as well as after 15 min of it soaking, a liquid metal sample was taken to detect the hydrogen content. The hydrogen content in the aluminium, after adding the metal Mg, amounted to 0.32 cm^3/100 g Al. Adding magnesium to the specified amount more than doubled the hydrogen content.

After a study of the Al-Sr addition, the hydrogen content in the initial sample of the aluminium melt amounted to 0.19 cm^3/100 g. Furthermore, the Al-Sr alloying addition was added to the melt in an amount equivalent to the strontium content in the metal (0.02%w). After the alloying addition's dilution, when the melt temperature reached 720ºC, as well as after 15 min of its soaking, a liquid metal sample was taken to detect the

hydrogen content. The hydrogen content in the aluminium after adding the Al-Sr alloying addition amounted to 0.23 cm^3/100 g Al. Adding strontium in the specified amounts contributed to an increase in the hydrogen content in the aluminium by 0.04 cm^3/100 g Al.

After a study of the Al-5%Ti-1%B addition, the hydrogen content in the initial sample of the aluminium melt amounted to 0.18 cm3/100 g Al. Furthermore, an Al-5%Ti-1%B alloying addition was added to the melt in the amount of 2.5 g. After the addition's dilution, when the melt temperature reached 720ºC, as well as after 15 min of its soaking, a liquid metal sample was taken to detect the hydrogen content. The hydrogen content in the aluminium after adding the alloying addition amounted to 0.20 cm^3/100 g Al. Adding the alloying addition in the specified amounts caused an increase in the hydrogen content in the aluminium of 0.02 cm^3/100g Al, which is within the measurement error [10–12].

CONCLUSIONS

The completed research revealed that the Ekoraf-F5 flux increases the hydrogen content in the Al melt by 0.19 cm^3/100 g, Ekoraf-F1 flux by 0.08 cm^3/100 g, FPR23 flux by 0.01 cm^3/100 g, Ti addition by 0.03 cm^3/100 g, Mn addition by 0.06 cm^3/100 g, Cu addition by 0.01 cm^3/100 g, Fe addition by 0.07 cm^3/100 g, Si addition by 0.05 cm^3/100 g, Mg addition by 0.17 cm^3/100 g, Al-Sr by alloying addition 0.04 cm^3/100 g, and Al-Ti-B alloying addition by 0.02 cm^3/100 g.

The maximum aluminium saturation with hydrogen was detected while applying refining fluxes and alloying additions containing alkali and alkaline earth metal halides, some of which forming crystalline hydrates. Fluxes containing hygroscopic and crystal water do not refine the metal and further saturate it with hydrogen.

In order to eliminate aluminum melt hydrogen absorption it is proposed:

to use only melt refining and cover-refining fluxes and completely reject the use of powder fluxes;

to ensure input control for fluxes and alloying additions and tighten control over fluxes' acceptance;

to store melt fluxes and alloying additives containing alkali and alkali earth metals halides under conditions eliminating their saturation with hygroscopic water; if necessary, to dry the fluxes before use;

to increase by 1.5-2 times the consumption of refining fluxes when preparing the aluminium-magnesium alloys.

The proposed activities will reduce the saturation of alloying additions and fluxes via the atmospheric moisture, decrease the consumption of flux per tonne of metal, and lessen the saturation of aluminum melts with hydrogen, which in the long run will reduce production cost and improve the quality the finished product.

ACKNOWLEDGEMENT

This paper is completed within the framework of Project 14.578.21.0193 "Development of theoretical and technological solutions for hydrogen reduction in the composition of aluminum and lean aluminum alloys" of the Federal Grant Program "Research and development in priority development trends of the Russian scientific and technological complex over 2014-2020" with financial support provided by the Ministry of Science and Education of the Russian Federation. Unique identifier of the Agreement RFMEFI57816X0193

REFERENCES

[1] Belyaev S.V., Kulikov B.P., Deev V.B., Baranov V.N., Rakhuba E.M. 2017. Analysis of Hydrogen Content in the Main Stages of Low-Alloy Aluminum Alloy Flat Ingot Manufacture, Metallurgist. 61(3-4): 325-329.

[2] Frolov V.F., Belyaev S.V., Gubanov I.Y. 2016. Influence of technological factors on the formation of structural defects in large ingots of aluminum alloys 1XXX Bulletin of the Magnitogorsk State Technical University. G.I. Nosov. 2: 24-28.

[3] Belyaev S.V., Baranov V.N., Gubanov I.Y. Kulikov B.P., Lisiv E. M., Bezrukikh A.I., Leonov V.V., Kirko V.I., Koptseva N.P. 2017. Saturation Dynamics of Aluminum Alloys with Hydrogen ARPN Journal of Engineering and Applied Sciences, November. 21: 6243-6247.

[4] Korolev S.P., Galushko A.M, Mikhaylovskiy V.M. 2011. Development and use of complex compounds to refine and modify aluminium alloys. Foundry and Metallurgy. 3(62): 51-57.

[5] Roučka J., Hotař J. 2015. Controlled Precipitation Gaseous Cavities in Aluminium Castings, Archives of Foundry Engineering. 15(4): 124-128.

[6] Brem V.V., Kozhukhar V.Ya., Dmitrenko I.V. 2009. Increase in moisture resistance of fluoride-oxide fluxes, Bulletin of Odessa Polytechnic University. 2: 197-204.

[7] Vetyukov M.M., Tsyplakov A.M., Shkolnikov S.N. 1987. Aluminum and magnesium electrometallurgy. Textbook for higher educational institutions, Metallurgy, Moscow.

[8] Kirko V.I., Dobrosmyslov S. S., Nagibin G. E., and Koptseva N. P. 2016. Electrophysical-mechanical properties of the composite SnO_2-Ag (Semiconductor-metal) ceramic material. ARPN Journal of Engineering and Applied Sciences. 11(1): 646-651.

[9] Uskov I.V., Belyaev S.V., Uskov D.I., Gilmanshina T.R., Kirko V.I., Koptseva N.P. 2016. Next-Generatiom Technologies of Manufacturing of Waveguides from Aluminum Alloys. ARPN Journal of Engineering and Applied Sciences. 11(21): 12367-12370.

[10] Yuriev Pavel O., Lesiv Elena M., Bezrukikh Alexander I., Belyaev Sergey V., Gubanov Ivan Y., Kirko Vladimir I., Koptseva Natalia P. 2016. Study of Change in the SCMS Strength Properties Depending on the Agueous-Clay Suspensions Concentration and Muscovites Amount in Its Composition. ARPN Journal of Engineering and Applied Sciences. 11(15): 9007-9012.

[11] Koptseva Natalia P. 2015. The current economic situation in Taymyr (the Siberian Arctic) and the prospects of indigenous peoples' traditional economy. Economic Annals-XXI. 9-10: 95-97.

[12] Moskalyuk Marina V., Koptseva Natalia P., Pimenova Natalia N., Sertakova Ekaterina A., Kharitonov Vladimir V. 2016. Study of air conditioning systems for storage and display of art works. ARPN Journal of Engineering and Applied Sciences. 11(23): 13878-13883.